Fabrication of high-photoresponsivity $BaSi_2$ films formed on conductive layers by radio-frequency sputtering

Ryota Koitabashi[1], Taira Nemoto[1], Masami Mesuda[2], Kaoru Toko[1], Takashi Suemasu[1*]
[1]*Institute of Applied Physics, University of Tsukuba, Tsukuba, Ibaraki 305-8573, Japan*
[2]*Tosoh Corporation, Advanced Materials Research Laboratory, Ayase, Kanagawa 252-1123, Japan*

We fabricated randomly-oriented polycrystalline $BaSi_2$ films on TiN metal layers by sputtering for the deployment of $BaSi_2$ solar cells on a flexible substrate. The formation of $BaSi_2$ films was demonstrated by X-ray diffraction and Raman spectroscopy. The photoresponsivity increased at wavelengths < 1000 nm, corresponding to the bandgap of $BaSi_2$, and reached 1.6 A/W at a wavelength of 650 nm under a bias voltage of 0.5 V applied to the front ITO electrode with respect to the TiN layers. This value is equivalent to the highest value ever achieved for undoped $BaSi_2$ epitaxial films by molecular beam epitaxy.

*Email: suemasu@bk.tsukuba.ac.jp

At present, crystalline-Si solar cells dominate the photovoltaics market, and are still the main technology.[1)] However, it is difficult to form them on flexible substrates because they are wafer-based. High-efficiency thin-film solar cells composed of chalcopyrite and cadmium telluride have been attracting much attention because they can be formed on glass substrates by cost effective growth procedure.[2-4)] Under such circumstances, we have paid special attention to semiconducting barium disilicide ($BaSi_2$) for Si-based thin-film solar cell applications.[5-7)] $BaSi_2$ consists of abundant Si and Ba, and has a large absorption coefficient ($\alpha = 3 \times 10^4$ cm^{-1} at 1.5 eV)[8-11)] and a large minority-carrier diffusion length of 10 μm.[12)] $BaSi_2$ also possesses a suitable band gap of 1.3 eV for a single junction solar cell.[9)] We have achieved energy conversion efficiencies approaching 10% in p-$BaSi_2$/n-Si heterojunction solar cells[13,14)] and demonstrated the operation of $BaSi_2$ homojunction solar cells on a Si substrate[15)] by molecular beam epitaxy (MBE). MBE is a very powerful technique to conduct fundamental studies such as the effect of Ba/Si atomic ratio on the electrical, optical, and defect properties in $BaSi_2$.[16-18)] It is, however, not a practical method for large-scale deployment. On the other hand, vacuum evaporation is a more feasible method. $BaSi_2$ films have been formed by vacuum evaporation on Si substrates using $BaSi_2$ granules,[19-24)] wherein a high carrier lifetime of 4.8 μs has been achieved.[21)] Sputtering is another large-area thin-film growth technique. We have formed $BaSi_2$ films on Si substrates by sputtering,[25-27)] and demonstrated very high photoresponsivity in C-doped $BaSi_2$ films equivalent to that in undoped $BaSi_2$ epitaxial films by MBE.[27)] As a next step, we explore the formation of $BaSi_2$ films on conductive layers for the deployment of $BaSi_2$ solar cells on flexible substrates. In this work, we chose indium-tin-oxide (ITO) and titanium nitride (TiN) as conductive layers, onto which we attempted to form $BaSi_2$ films. ITO is well known as transparent conductive oxide. TiN has a good chemical stability and a strong resistance against heating.[29,30)] Therefore, it is often used to protect surfaces. Thanks to a low resistivity of 10^{-5}–10^{-4} Ωcm for TiN, it can be used as an electrode.[31,32)] We investigated the photoresponsivity of $BaSi_2$ films formed by sputtering on ITO or TiN layers.

We used a 2-inch-diameter polycrystalline $BaSi_2$ target manufactured by Tosoh Corporation. 2 pieces of platelike Ba sources (1.0 cm × 2.0 cm) were placed on the $BaSi_2$ target to satisfy the stoichiometry of a Ba/Si atomic ratio in grown films.[25,26)] First, we

fabricated 200 nm-thick ITO layers or 250 nm-thick TiN layers on a high-resistivity floating-zone (FZ) Si substrates (ρ > 1000 Ωcm) by sputtering at different temperatures (T_{cond}). After that, $BaSi_2$ films were formed at a substrate temperature (T_S) of 500–600 °C by a helicon-wave excited plasma sputtering system (ULVAC MB 00-1040). The Ar pressure was set at 0.5 Pa and the radio-frequency power was kept at 50 W. After the formation of $BaSi_2$ films, a 3 nm-thick amorphous Si (a-Si) capping layer was deposited by sputtering in situ for surface passivation.[13,33] Finally, ITO electrodes with a diameter of 1 nm and a thickness of 80 nm were made on the front surface. Surface morphologies of ITO and TiN layers were observed by optical microscopy. The crystalline quality of grown layers were measured using grazing-incidence (GI) 2θ X-ray diffraction (XRD; Rigaku Smart Lab) with a Cu Kα radiation source and Raman spectroscopy (JASCO NRS-5100) equipped with a frequency-doubled Nd:YAG laser (532 nm, 5.1 mW). The photoresponse spectra were evaluated with the use of a lock-in technique using a xenon lamp and a single monochromator with a focal length of 25cm (Bunko Keiki SM-1700A and RU-60N). All the measurements were performed at room temperature. Details of the samples preparation are summarized in Table I.

Table I. Sample preparation details: deposition temperature for ITO and TiN layers (T_{cond}), their layer thicknesses (d_{cond}), temperature for $BaSi_2$ deposition (T_S), $BaSi_2$ layer thickness (d_{BaSi2}), and a-Si layer thickness ($d_{a\text{-}Si}$) are specified.

Sample	T_{cond} (°C)	d_{cond} (nm)	T_S (°C)	d_{BaSi2} (nm)	$d_{a\text{-}Si}$ (nm)
ITO-1	RT	200	-	-	-
ITO-1’	RT	200	600	-	-
ITO-2	RT	200	500	530	3
ITO-3	RT	200	550	540	3
ITO-4	RT	200	575	490	3
ITO-5	RT	200	600	590	3
TiN-1	100	250	-	-	-
TiN-2	150	250	-	-	-

TiN-3	200	250	-	-	-
TiN-1’	100	250	600	-	-
TiN-2’	150	250	600	-	-
TiN-3’	200	250	600	-	-
TiN-4	100	250	600	290	3
TiN-5	150	250	600	240	3

Optical micrograph of the surface of sample ITO-1 is shown in Fig. 1(a). The surface of this sample was flat. We heated this sample up to 600 °C to see what would happen. This is because we need to set T_S at 600 °C upon the formation of $BaSi_2$ films by sputtering.[25-27] We see the change in color and aggregates on the surface of sample ITO-1’. The electron concentration was increased from 6.0×10^{19} in sample ITO-1 to 1.9×10^{21} cm^{-3} in sample ITO-1’. The resistivity of the ITO films was also drastically changed from 1.1×10^{-2} to 1.7×10^{-4} Ωcm after this high-temperature process. The GI-XRD patterns in Fig. 1(b) show that the crystallization of ITO films was promoted in sample ITO-1’. Figure. 1(c) shows the Raman spectra of $BaSi_2$ films in samples ITO-2–5. Peaks denoted by A_g, E_g, and F_g originate from Si tetrahedra in the lattice of $BaSi_2$.[34] However, their peak intensities decreased with increasing T_S. A peak at 503 cm^{-1}, marked as α, became intense, probably due to the oxidation of $BaSi_2$ films caused by the diffusion of O atoms from the ITO underlayers. We ascribed this Raman line to substances such as Ba oxides[35] and Si gel.[36] In sample ITO-5 (T_S = 600 °C), there was no Raman line related to $BaSi_2$. Similar result was reported when the formation of $BaSi_2$ films was attempted on a SiO_2 substrate.[28] Another peak marked as β also appeared in sample ITO-2 (T_S = 500 °C). The origin of this line was not made clear at present. The photoresponsivity of the $BaSi_2$ films in samples ITO-2–5 was quite small even under large bias voltages (V_{bias}) applied between the front ITO electrode and the ITO layers beneath the $BaSi_2$ films. Based on these results, we conclude that it is difficult to form $BaSi_2$ films on ITO layers without forming oxides.

Figure 2(a) shows the optical micrographs of samples TiN-1(1’)–3(3’). The surfaces of samples TiN-1 (T_{cond} = 100 °C) and TiN-2 (T_{cond} = 150 °C) were flat. In contrast, the surface of sample TiN-3, prepared at T_{cond} = 200 °C, was rough due to the

aggregation of formed TiN. We heated these samples up to 600 °C in TiN-1'–3'. There was not so much difference in the surface morphology in all the samples TiN-1'–3' after the high-temperature process. Figure 2(b) shows the GI-XRD patterns of TiN films in samples TiN-1'–3'. In samples TiN-1' and TiN-2', diffraction peaks of 111, 220, and 311 of TiN were observed.[37] On the other hand, for TiN films in sample TiN-3', 200 and 222 peaks were added, differently from those deposited at $T_{cond} \leq 150$ °C in samples TiN-1' and TiN-2'.[38] According to Ref. 39, the crystal orientation of TiN is sensitive to its Si content. Thereby there is a possibility that higher T_{cond} (200 °C) for sample TiN-3' would promote the diffusion of Si atoms from the Si substrate into the grown layers. The resistivity of samples TiN-1'– 3' was about 2–3 × 10^{-4} Ωcm.

Raman spectra of grown layers in samples TiN-4 (T_{cond} =100 °C) and TiN-5 (T_{cond} =150 °C) are shown in Fig. 3(a). All the obtained Raman lines originated from Si tetrahedra in $BaSi_2$, differently from those marked as α and β in samples ITO-2–5 in Fig. 1(c). The GI-XRD patterns of samples TiN-4 and TiN-5 observed are compared with those calculated from the crystal structure of orthorhombic $BaSi_2$ in Fig. 3(b). Almost all the diffraction peaks in these samples coincide with those calculated, meaning that $BaSi_2$ films were randomly oriented on the TiN layers.

Figure 4 shows the photoresponse spectra of $BaSi_2$ films in sample TiN-5 under different values of V_{bias} applied to the front ITO electrode with respect to the TiN layers beneath the $BaSi_2$ films. The photoresponsivity increased sharply at wavelengths shorter than approximately 1000 nm, corresponding to the band gap of $BaSi_2$. The photoresponsivity increased with V_{bias}, and reached 1.6 A/W at a wavelength of approximately 650 nm at V_{bias} = 0.5 V. The obtained photoresponsivities are as high as those obtained for undoped $BaSi_2$ epitaxial films by MBE. The photoresponsivity of 0.45 A/W at V_{bias} = 0.1 V in Fig. 4 is equivalent to the highest value ever achieved for undoped $BaSi_2$ epitaxial films by MBE (0.50 A/W at V_{bias} = 0.1 V).[40] On the basis of these results, we succeeded to form high-photoresponsivity $BaSi_2$ films on conductive layers for the first time. There are still two issues to be addressed. For one thing we are not sure for certain why such randomly oriented $BaSi_2$ films exhibited such high photoresponsivity. For another thing, we employed Si substrates in this work. Since we used a sputtering

system equipped with radiation heating to raise the substrate temperature, it was difficult to raise the temperature of transparent SiO_2 substrates up to 600 °C necessary for the formation of $BaSi_2$ films in the present system. We have to modify the way of heating substrates soon. It was reported in Ref. 41 that 80-nm-thick TiN layers worked as a diffusion barrier against O atoms from SiO_2 substrates. We therefore expect the formation of high-photoresponsivity $BaSi_2$ films on a TiN/SiO_2 substrate by sputtering.

In summary, we formed $BaSi_2$ films by sputtering on conductive layers such as ITO and TiN layers to explore the possible deployment of $BaSi_2$ solar cells on a flexible substrate. In the case of ITO layers, Raman spectroscopy revealed that $BaSi_2$ films got oxidized and thus the photoresponsivity was quite small. In contrast, we succeeded to form $BaSi_2$ films on TiN layers deposited at 100 and 150 °C, and achieved high photoresponsivity reaching 1.6 A/W at a wavelength of 650 nm at V_{bias} = 0.5 V. This value is equivalent to the highest value ever obtained for undoped $BaSi_2$ epitaxial films by MBE. These results convince us that sputtering is a promising method to form high-photoresponsivity $BaSi_2$ films on a large-area substrate.

Acknowledgments

This work was financially supported by the Japan Society for the Promotion of Science (JSPS) KAKENHI (Grant No. 18H03767). We express thanks to Ms. T. Tawara and Mr. S. Tanigawa for their help at the Nanotechnology Platform of the University of Tsukuba.

Figures

Figure 1. (a) Optical micrographs of ITO films for samples ITO-1 (T_{cond} = RT) and those after the high-temperature process (T_S = 600 °C) for samples ITO-1'. (b) GI-XRD patterns of samples ITO-1 and ITO-1'. (c) Raman spectra of samples ITO-2–5 with $BaSi_2$ films deposited at T_S = 500, 550, 575, and 600 °C, respectively. Peaks denoted by A_g, E_g, and F_g originate from Si tetrahedra in $BaSi_2$.

Figure 2. (a) Optical micrographs of TiN films in samples TiN-1–3 with TiN layers deposited at T_{cond} =100, 150, and 200 °C, respectively, and those after the high-temperature process (T_S = 600 °C) for samples TiN-1'–3'. (b) GI-XRD patterns of samples TiN-1'–3'.

Figure 3. (a) Raman spectra of $BaSi_2$ films in samples TiN-4 and TiN-5, wherein TiN layers were deposited at T_{cond} =100 and 150 °C, respectively, and $BaSi_2$ films were formed at T_S = 600 °C. (b) GI-XRD patterns of samples TiN-4, TiN-5, and those calculated.

Figure 4. Photoresponse spectra of $BaSi_2$ films in sample TiN-5 (T_{cond} = 150 °C, T_S = 600 °C) under a bias voltage of 0–0.5 V applied to the front ITO electrode with respect to the TiN films.

Reference

1) K. Yoshikawa, H. Kawasaki, W. Yoshida, K. Konishi, K. Nakano, T. Uto, D. Adachi, M. Kakematsu, H. Uzu, and K. Yamamoto, Nat. Energy **2**, 17032 (2017).

2) P. Jackson, R. Wuerz, D. Hariskos, E. Lotter, W. Witte, and M. Powalla, Phys. Status Solidi Rapid Research Lett. **10**, 583 (2016).

3） M. A. Green, Prog. Photovolt. **26**, 427 (2017).

4) A. Kanevce, M. O. Reese, T. M. Barnes, S. A. Jensen, and W. K. Metzger, J. Appl. Phys. **121**, 214506 (2017).

5) T. Suemasu, Jpn. J. Appl. Phys. **54**, 07JA01 (2015).

6) T. Suemasu and N. Usami, J. Phys. **D 50**, 023001 (2017).

7) M. Kumar, N. Umezawa, and M. Imai, Jpn. J. Appl. Phys. **59**, SF0803 (2020).

8) D. B. Migas, V. L. Shaposhnikov, and V. E. Borisenko, Phys. Status Solidi **B 244**, 2611 (2007).

9) K. Toh, T. Saito, and T. Suemasu, Jpn. J. Appl. Phys. **50**, 068001 (2011).

10) M. Kumar, N. Umezawa, and M. Imai, Appl. Phys. Express **7**, 071203 (2014).

11) M. Kumar, N. Umezawa, and M. Imai, J. Appl. Phys.**115**, 203718 (2014).

12) M. Baba, K. Toh, K. Toko, N. Saito, N. Yoshizawa, K. Jiptner, T. Sakiguchi, K. O. Hara, N. Usami, and T. Suemasu, J. Cryst. Growth **348**, 75 (2012).

13) S. Yachi, R. Takabe, K. Toko, and T. Suemasu, Appl. Phys. Lett. **109**, 072103 (2016).

14) T. Deng, T. Sato, Z. Xu, R. Takabe, S. Yachi, Y. Yamashita, K. Toko, and T. Suemasu, Appl. Phys. Express **11**, 062301 (2018).

15) K. Kodama, Y. Yamashita, K. Toko, and T. Suemasu, Appl. Phys. Express **12**, 041005 (2019).

16) R. Takabe, T. Deng, K. Kodama, Y. Yamashita, T. Sato, K. Toko, and T. Suemasu, J. Appl. Phys. **123**, 045703 (2018).

17) Y. Yamashita, T. Sato, K. Toko, A. Uedono, and T. Suemasu, Appl. Phys. Express 12, 055506 (2019).

18) S. Sugiyama, Y. Kimura, Y. Yamashita, K. Toko, N. Usami, and T. Suemasu, Jpn. J. Appl. Phys. **59**, SFFA04 (2020).

19) K. O. Hara, Y. Nakagawa, T. Suemasu, and N. Usami, J. Appl. Phys. **54**, 07JE02 (2015).

20) K. O. Hara, C. T. Trinh, K. Arimoto, J. Yamanaka, K. Nakagawa, Y. Kurokawa, T. Suemasu, and N. Usami, J. Appl. Phys. **120**, 045103 (2016).
21) C. T. Trinh, Y. Nakagawa, K. O. Hara, R. Takabe, T. Suemasu, and N. Usami, Mater. Res. Express **3**, 076204 (2016).
22) T. Yoshino, Y. Nakagawa, Y. Kimura, M. Fujiwara, Y. Kurokawa, and N. Usami, Jpn. J. Appl. Phys. 59, SFFA10 (2020).
23) Y. Kimura, M. Fujiwara, Y. Nakagawa, K. Gotoh, Y. Kurokawa, and N. Usami, Jpn. J. Appl. Phys. 59, SFFA05 (2020).
24) K. O. Hara, K. Arimoto, J. Yamanaka, and K. Nakagawa, Jpn. J. Appl. Phys. 59, SFFA02 (2020).
25) S. Matsuno, R. Takabe, S. Yokoyama, K. Toko, M. Mesuda, H. Kuramochi, and T. Suemasu, Appl. Phys. Express **11**, 071401 (2018).
26) S. Matsuno, T. Nemoto, M. Mesuda, H. Kuramochi, K. Toko, and T. Suemasu, Appl. Phys. Express **12**, 021004 (2019).
27) T. Nemoto, S. Matsuno, T. Sato, K. Gotoh, M. Mesuda, H. Kuramochi, K. Toko, N. Usami, and T. Suemasu, Jpn. J. Appl. Phys. **59**, SFFA06(2020).
28) K. Morita, Y. Inomata, and T. Suemasu, Thin Solid Films **508**, 363 (2006).
29) V. Chawla, R. Jayaganthan, and R. Chandra, Mater. Charat, **59**, 1015 (2008).
30) M. A. Jithin, K. L. Ganapathi, G. N. V. R. Vikram, N. K. Udayashankar, and S. Mohan, Sens. Actuator A Phys. **272** ,199 (2018).
31) F. Vaz, J. Ferreira, E. Ribeiro, L. Rebouta, S. Lanceros Méndeza, J. A. Mendes, E. Alves, Ph. Goudeau, J. P. Rivièrec, F. Ribeiro, I. Moutinho, K. Pischow, and J.de Rijk, Surf. Coat, technol. **191**, 317 (2005).
32) G. Lemperière, J. M. Poitevin, Thin Solid Films **3**, 339 (1984).
33) R. Takabe, S. Yachi, W. Du, D. Tsukahara, H. Takeuchi, K. Toko, and T. Suemasu AIP Advances **6**, 085107 (2016).
34) H. Hoshida, T. Suemasu, and Y. Terai, Defect and Diffusion Forum **386**, 43 (2018).
35) B. Hruška, A. A. Osipov, L. M. Osipova, M. Chromčíková, J. Macháček and M. Liška, Vib. Spectrosc. **105**, 102970 (2019).

36) K. Chen, Z. Bao, J. Shen, G. Wu, B. Zhou, and K. H. Sandhage, J. Mater. Chem. **22**, 16196 (2012).

37) P. LeClair, Thin Solid Films **376**, 9 (2000).

38) P. Patsalas, C. Charitidis, S. Logothetidis, Surf. Coat, technol.**125**, 335 (2000).

39） M. Diserens, Surf. Coat, technol.**108**, 241 (1998).

40） Y. Yamashita, T. Sato, N. Saitoh, N. Yoshizawa, K. Toko, and T. Suemasu, J. Appl. Phys. **126**, 215301 (2019).

41) K. G. Grigorov, G. I. Grigorov, M. V. Stoyanova, R. A. Chakalov, J. L. Vignes, J. P. Langeron, P. Denjean, and J. Perriere, Vacuum **44**, 1119 (1993).

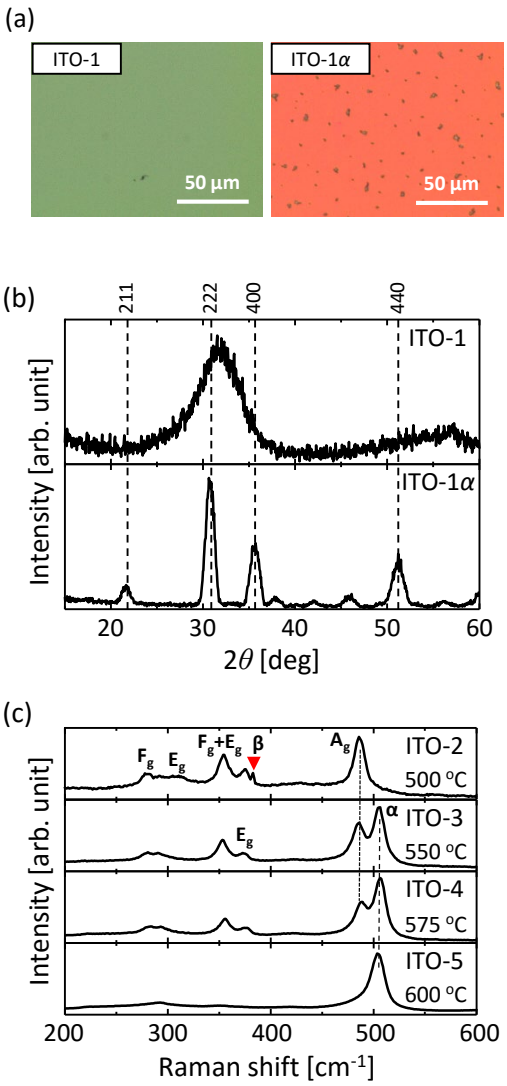
(a)
ITO-1
50 μm
ITO-1α
50 μm
(b)
211
222
400
440
ITO-1
ITO-1α
Intensity [arb. unit]
20
30
40
50
60
2θ [deg]
(c)
Fg
Eg
Fg+Eg
β
Ag
ITO-2
500 °C
α
ITO-3
550 °C
Eg
ITO-4
575 °C
ITO-5
600 °C
Intensity [arb. unit]
200
300
400
500
600
Raman shift [cm-1]

Fig. 1

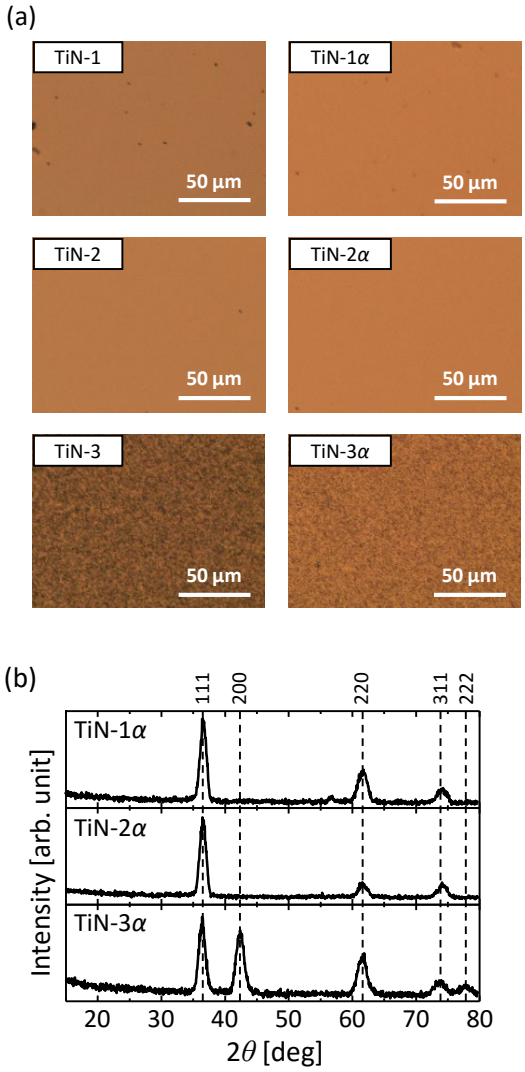
(a)
TiN-1
50 µm
TiN-1α
50 µm
TiN-2
50 µm
TiN-2α
50 µm
TiN-3
50 µm
TiN-3α
50 µm
(b)
111
200
220
311
222
TiN-1α
TiN-2α
TiN-3α
Intensity [arb. unit]
20
30
40
50
60
70
80
2θ [deg]

Fig. 2

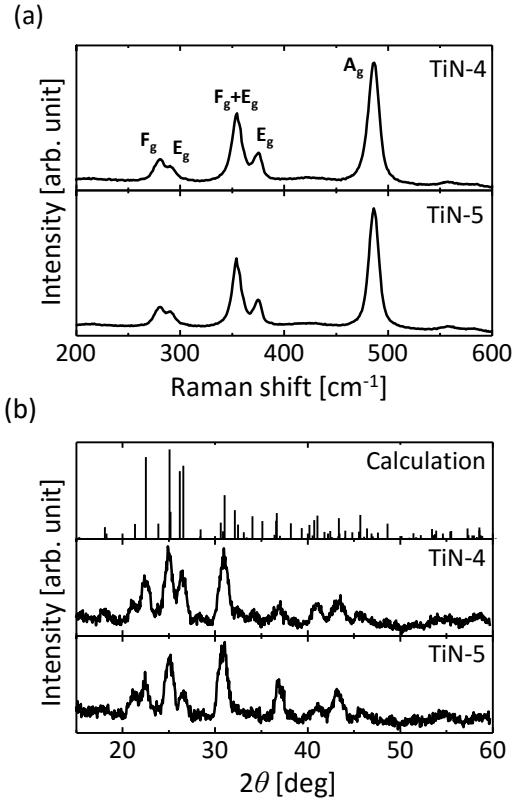
(a)
TiN-4
TiN-5
A_g
F_g+E_g
F_g
E_g
E_g
Intensity [arb. unit]
200
300
400
500
600
Raman shift [cm^{-1}]
(b)
Calculation
TiN-4
TiN-5
Intensity [arb. unit]
20
30
40
50
60
2θ [deg]

Fig. 3

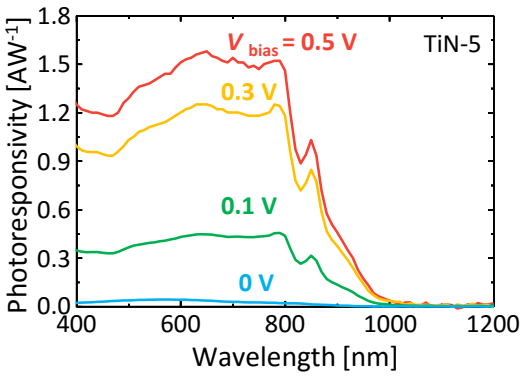
Photoresponsivity [AW-1]
1.8
1.5
1.2
0.9
0.6
0.3
0.0
400
600
800
1000
1200
Wavelength [nm]
V bias = 0.5 V
0.3 V
0.1 V
0 V
TiN-5

Fig. 4